Electronic Supplementary Material (ESI) for Journal of Materials Chemistry A.

Supporting Information

Ice crystal-assisted intercalation of PANI within $Ti_3C_2T_x$ MXene thin-films for flexible supercapacitor electrodes with simultaneously high mechanical strength and rate performance

Jianhua Wang,[a1] Degang Jiang,[a, b1] Maozhuang Zhang,[a] Yuesheng Sun,[a] Mingyuan Jiang,[a] Yiqi Du,[a] Jingquan Liu [a*]*

[a] College of Materials Science and Engineering, Institute for Graphene Applied Technology Innovation, Qingdao University, Ningxia Road 308 Qingdao 266071, China.

[b] Institute for Frontier Materials, Deakin University, Geelong, VIC 3216, Australia

*Corresponding author. E-mail: jliu@qdu.edu.cn (J. Liu), djiang@deakin.edu.au (D. Jiang)

[1] These authors contributed equally to this work.

Regents

All chemicals were used as received without further purification. MAX (Ti_3AlC_2, 400 mesh) was purchased from Jilin Eleven Technology Co., Ltd. Ammonium persulfate (APS) was from Shanghai Jizhi Biochemical Technology Co., Ltd. Aniline monomer was from Shanghai Wokai Biotechnology Co., Ltd. Polyvinyl alcohol (PVA) was supplied by Shanghai Aladding Biochemical Technology Co., Ltd. Lithium fluoride (CP), ethanol absolute (AR) and hydrochloric acid (AR) were received from Sinopharm Chemical Reagent Co., Ltd. Distilled water was prepared using a Flom ultrapure water system.

Characterizations

The morphologies of the samples were observed by using a field emission scanning electron microscope (SEM, JEOL 6701, Japan) and atomic Force Microscope (AFM, Keysight 5500). TEM images were obtained using a JEM-2100F electron microscope with an accelerating voltage of 200Kv. The morphology and structure of the samples were investigated with energy dispersive X-ray spectrometer. The XPS spectra of the prepared samples were examined by Thermo ESCALAB 250XI X-ray photoelectron spectrometer (XPS, Physical Electronics, USA). The structures of the as-prepared samples were analyzed with XRD (DX2700, China) at a scan rate (2θ) of 5^o min^{-1} ranging from 4^o to 80^o, operating at Cu Kα radiation (l=1.5418 Å) with an accelerating voltage of 40 kV and an applied current of 30 mA. Fourier transform infrared (FT-IR) spectroscopy was measured on Nicolet iN10MX Fourier infrared spectrometer. The Raman spectrum was analyzed by a micro-Raman spectrometer (DXR2), and the

irradiation source was a 633 nm laser. Thermogravimetric analysis (TGA) was performed under nitrogen at 35-800℃ using a thermogravimetric analyzer (TG 209 F3). All the electrochemical tests were performed using a CHI 760E electrochemical workstation.

Calculations

Gravimetric specific capacitance (C_g) of all electrodes in a three electrodes system was calculated through the following equation:

$$C_g = \frac{I\Delta t}{m\Delta U} \quad (1)$$

Where I is the current density, ΔU is the potential window, Δt is the discharge time (s), and m is the mass of each electrode.

Volume specific capacitance (C_v) of all electrodes in a three electrodes system was calculated through the following equation:

$$C_v = \frac{I\Delta t}{V\Delta U} \quad (2)$$

Where I is the current density, ΔU is the potential window, Δt is the discharge time (s), and V is the volume of each electrode sheet.

The specific capacitances of the compressible supercapacitor were calculated from their GCDs which were carried out on symmetrical supercapacitor systems according to the following equation:

$$C = \frac{2I\Delta t}{m\Delta U} \quad (3)$$

Where C is the specific capacitance (A g^{-1}), I is the discharge current (A), Δt is the discharge time (s), m (g) is the mass of a single MGC hybrid electrode and ΔU is the voltage window (V).

The energy density and power density of symmetrical supercapacitor systems were calculated using the following equations:

$$E = \frac{C_t \Delta U^2}{2 \times 3.6} \quad (4)$$

$$P = \frac{E}{t} \quad (5)$$

Where E (Wh kg^{-1}) is the energy density, P (W kg^{-1}) is the power density of the symmetrical supercapacitor system, C_t (A g^{-1}) is the specific capacitance of the whole symmetrical supercapacitor system, which is equal to C/2. ΔU (V) is the voltage window, and t (h) is the discharge time, respectively.

The real C′(ω) and imaginary part C″(ω) capacitances can be calculated by the following formulas：

$$C'(\omega) = \frac{-Z''(\omega)}{\omega\left|Z(\omega)^2\right|} \quad (6)$$

$$C''(\omega) = \frac{Z'(\omega)}{\omega\left|Z(\omega)^2\right|} \quad (7)$$

where ω is the angular frequency, Z′(ω) and Z″(ω) is the real and imaginary parts of the Z(ω), respectively.

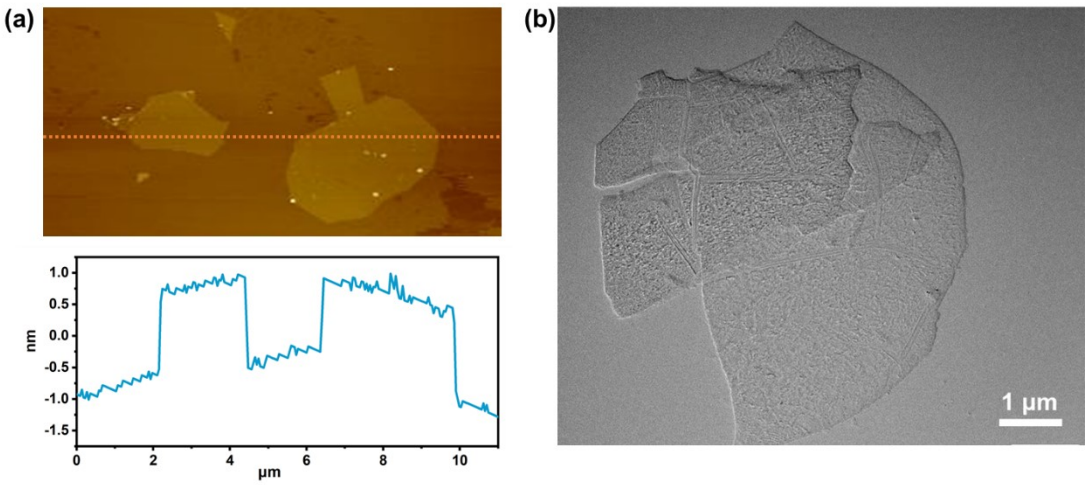

Fig. S1. (a) AFM image and height file of MXene. (b) TEM image of MXene.

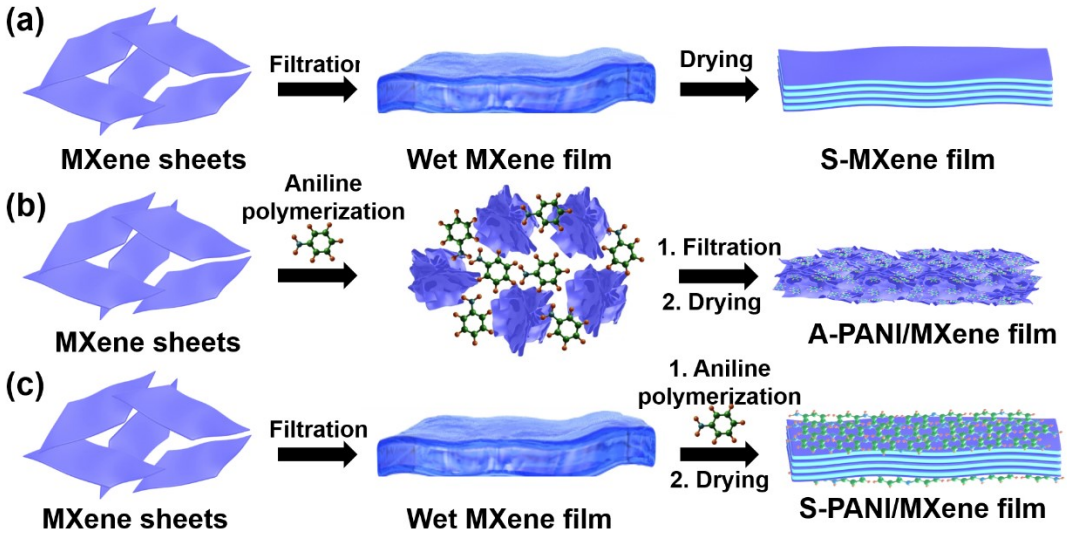

Fig. S2. Schematic illustration for the preparation process of (a) conventional stacked pure MXene film (S-MXene), (b) aggregated polyaniline/MXene film (A-PANI/MXene), and (c) stacked PANI/MXene film (S-PANI/MXene).

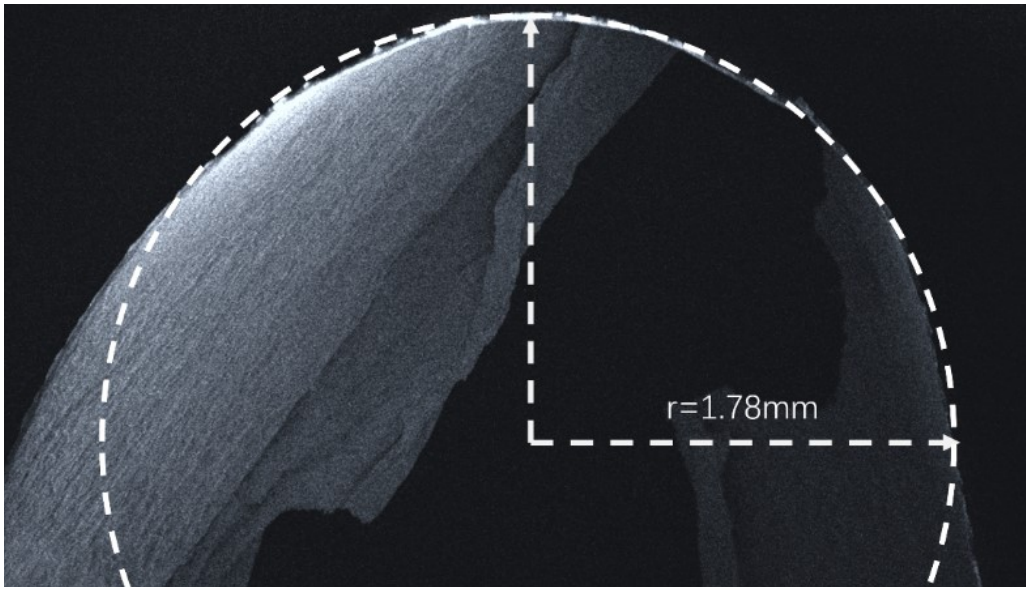

Fig. S3. SEM image of the I-PANI/MXene film folded with a small bending radius (1.78 mm).

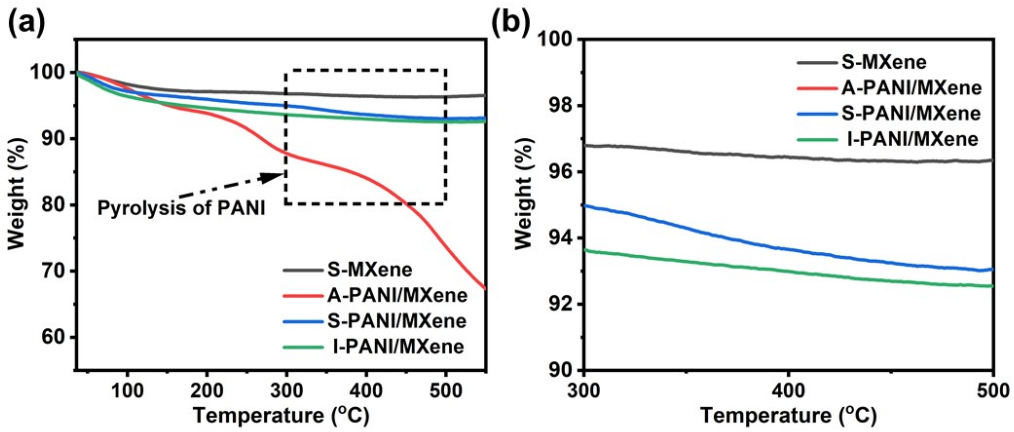

Fig. S4. (a) Thermogravimetric analysis (TGA) curves of S-MXene, A-PANI/MXene, S-PANI/MXene, and I-PANI/MXene films. (b) Magnified regions of the curves at 300 to 500 °C.

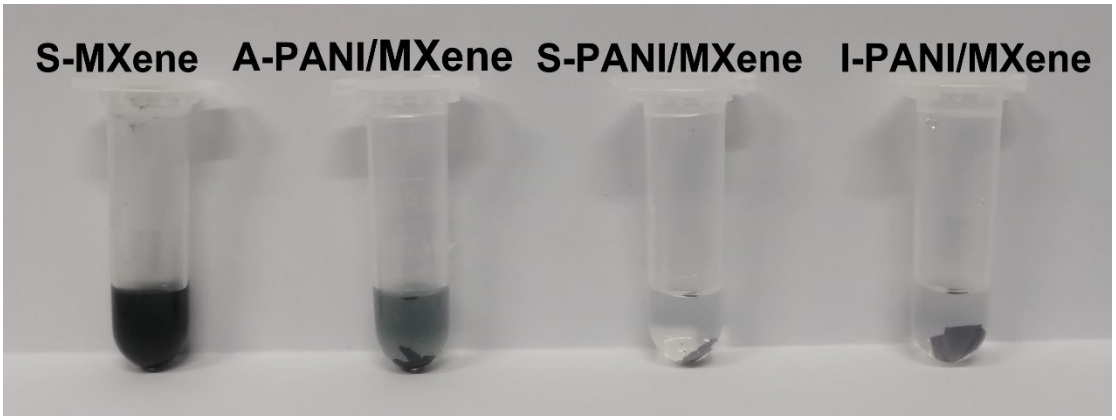

Fig. S5. Photo images showing the ultrasonic resistance of S-MXene, A-PANI/MXene, S-PANI/MXene, and I-PANI/MXene films after 5 min of sonication.

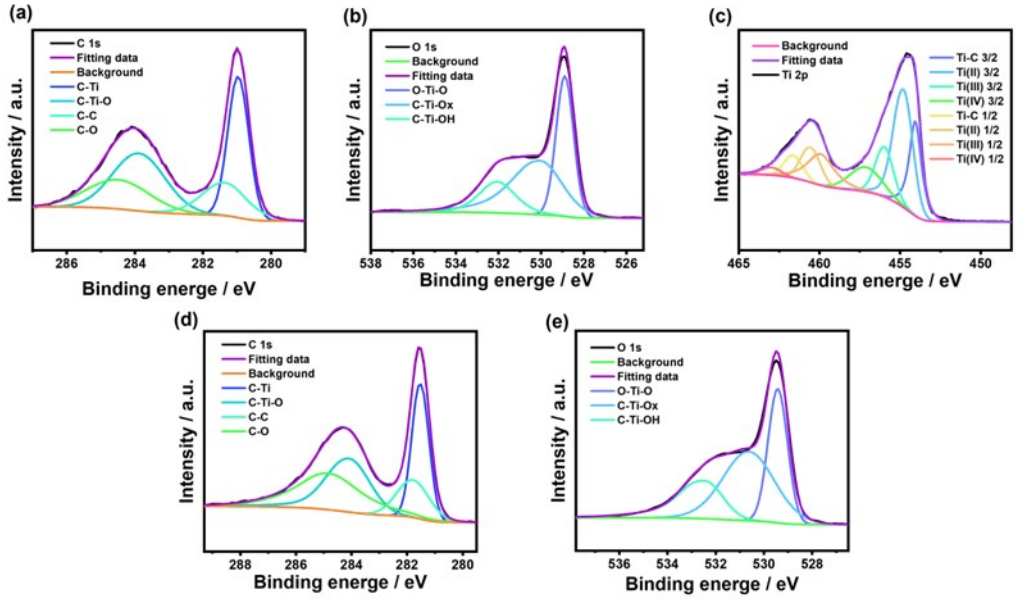

Fig. S6. High-resolution XPS spectra of (a) C 1s, (b) O 1s and (c) Ti 2p spectra for I-PANI/MXene film. High-resolution XPS spectra of (d) C 1s and (e) O 1s spectra for S-MXene film.

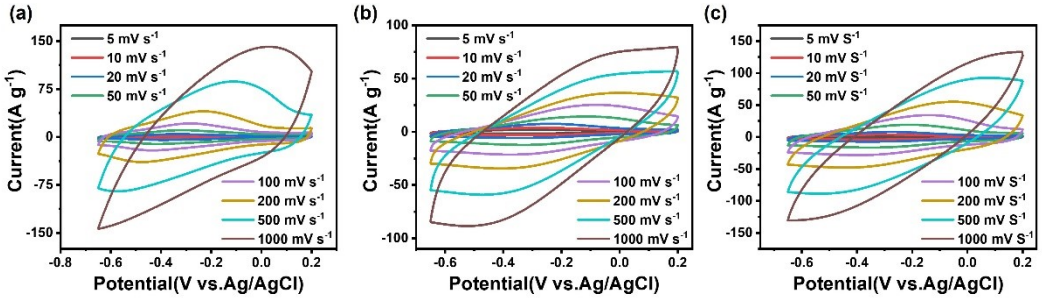

Fig. S7. CV curves of (a) S-MXene, (b) A-PANI/MXene, and (c) S-PANI/MXene film electrode at scan rate from 5 to 1000 mV s^{-1}.

Table S1. Comparisons of electrochemical performances of this work and those reported from literatures.

Electrode materials	Capacitance	Capacitance retention	Ref.
Ti_3C_2Tx FSC	214 μF cm^{-2} at 5 mV s^{-1}	101 μF cm^{-2} at 100 mV s^{-1} (50%)	1
IDT@rGO	345.5 F g^{-1} at 0.6 A g^{-1}	293.6 F g^{-1} at 5.3 A g^{-1} (84.95%)	2
ZIHC	318 μF cm^{-2} at 5 mV s^{-1}	105 μF cm^{-2} at 200 mV s^{-1} (33%)	3
$PANI_{0.7}$/MXene	560 μF cm^{-2} at 5 mV s^{-1}	360 μF cm^{-2} at 100 mV s^{-1} (64%)	4
MXene/rGO 1：99	245 μF cm^{-2} at 2 mV s^{-1}	193 μF cm^{-2} at 100 mV s^{-1} (76%)	5
GM_2	920 μF g^{-1} at 5 mV s^{-1}	124 μF g^{-1} at 500 mV s^{-1} (15%)	6
MXene/CN	113 F g^{-1} at 5 mV s^{-1}	38 F g^{-1} at 300 mV s^{-1} (33.6%)	7
Ti_3C_2Tx and VN/PC	197 F g^{-1} at 1 A g^{-1}	50 F g^{-1} at 10 A g^{-1} (25.4%)	8
d-Ti_3C_2Tx	73 mF cm^{-2} at 10 mV s^{-1}	46 mF cm^{-2} at 200 mV s^{-1} (36%)	9
Ti_3C_2/ZnO	200 F cm^{-3} at 2 mV s^{-1}	149 F cm^{-3} at 100 mV s^{-1} (74.5%)	10
MXene	307 F g^{-1} at 20 mV s^{-1}	225 F g^{-1} at 100 mV s^{-1} (73.2%)	11
MXene	405 F g^{-1} at 1 A g^{-1}	281 F g^{-1} at 20 A g^{-1} (70%)	12
I-PANI/MXene	1360 F cm^{-3} And 385 F g^{-1} at 5 mV s^{-1}	343 F g^{-1} at 100 mV s^{-1} (89%) 321 F g^{-1} at 500 mV s^{-1} (83.3%) 312 F g^{-1} at 1000 mV s^{-1} (81%) 263 g^{-1} at 5000 mV s^{-1} (68.3%) 207 F g^{-1} at 10000 mV s^{-1} (53.9%)	This work

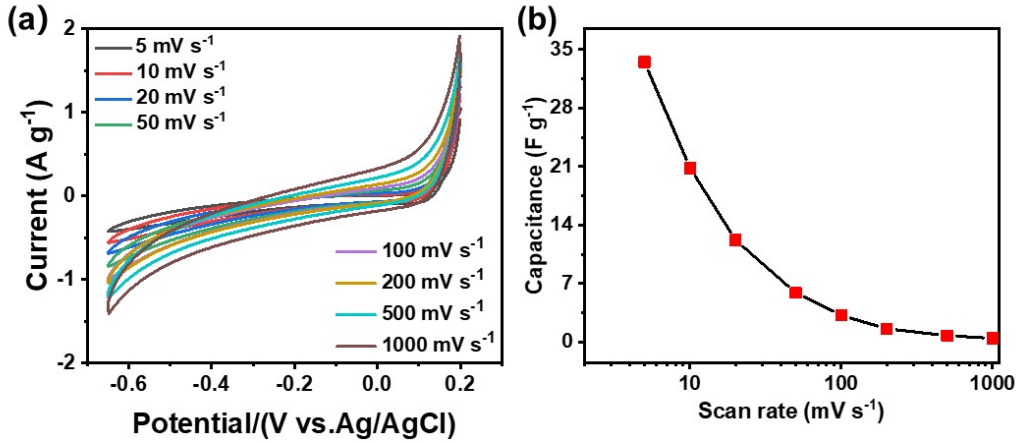

Fig. S8 (a) CV curves and (b) specific capacitance of pure PANI electrode at a scan rate from 5 to 1000 mV s^{-1}.

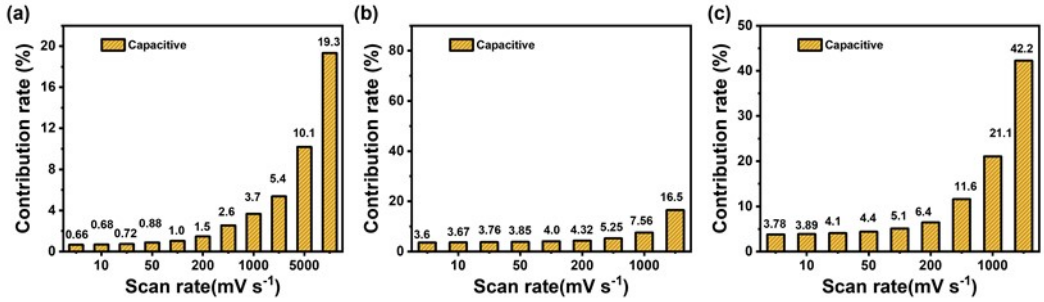

Fig. S9. Capacitive contributions of a) S-MXene, (b) A-PANI/MXene, and (c) S-PANI/MXene electrodes at different scan rates.

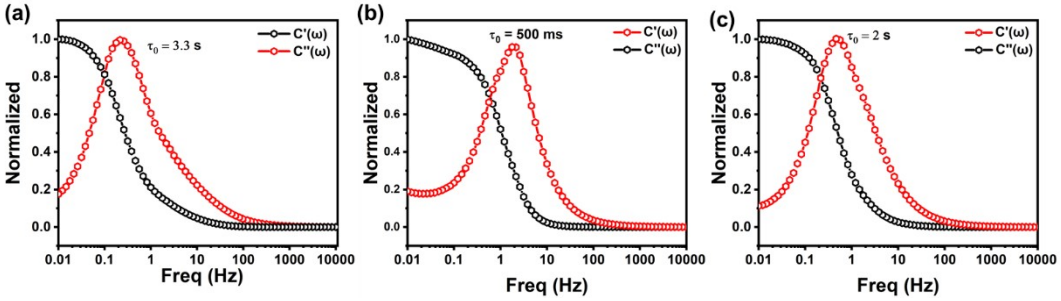

Fig. S10. Normalized real and imaginary capacitances of (a) S-MXene, (b) A-

PANI/MXene, and (c) S-PANI/MXene electrode.

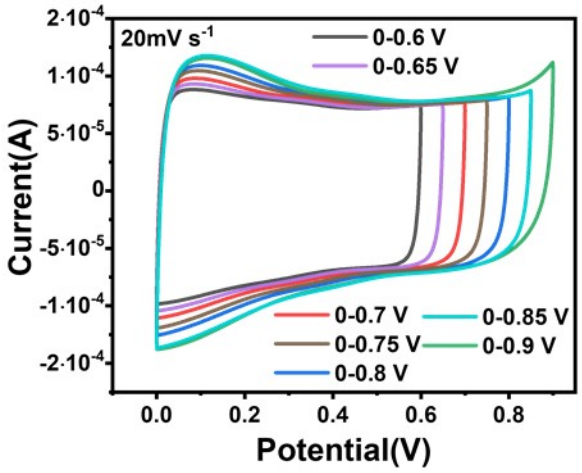

Fig. S11. The CV curves of I-PANI/MXene devices in different voltage windows at 20 mV s^{-1}

References

1. B. Shi, Li, A. Chen, T. C. Jen, X. Liu and G. Shen, *Nanomicro Lett*, 2021, **14**, 34.
2. Y. Xu, B. Pan, W. S. Li, L. Dong, X. Wang and F. G. Zhao, *ACS Appl Mater Interfaces*, 2021, **13**, 41537-41544.
3. L. Huang, Y. Lin, W. Zeng, C. Xu, Z. Chen, Q. Wang, H. Zhou, Q. Yu, B. Zhao, L. Ruan and S. Wang, *Langmuir*, 2022, **38**, 5968-5976.
4. Y. Wang, X. Wang, X. Li, Y. Bai, H. Xiao, Y. Liu and G. Yuan, *Chem. Eng. J.*, 2021, **405**, 126664.
5. A. M. Navarro-Suárez, K. Maleski, T. Makaryan, J. Yan, B. Anasori and Y. Gogotsi, *Batteries Supercaps*, 2018, **1**, 33-38.
6. S. Saha, K. Arole, M. Radovic, J. L. Lutkenhaus and M. J. Green, *Nanoscale*, 2021, **13**, 16543-16553.
7. H. Hwang, S. Byun, S. Yuk, S. Kim, S. H. Song and D. Lee, *Appl. Surf. Sci.*, 2021, **556**, 149710.
8. S. Venkateshalu and A. N. Grace, *Electrochim. Acta*, 2020, **341**, 136035.
9. L. Weng, F. Qi and Y. Min, *Mater. Lett.*, 2020, **278**, 128235.
10. F. Wang, M. Cao, Y. Qin, J. Zhu, L. Wang and Y. Tang, *RSC Adv.*, 2016, **6**, 88934-88942.
11. J. B. Lee, G. H. Choi and P. J. Yoo, *J. Alloys Compd.*, 2021, **887**, 161034.
12. T. Guo, D. Zhou, L. Pang, M. A. Darwish and Z. Shi, *Scr. Mater.*, 2022, **213**, 114590.